IEEE Photonics Journal
An IEEE Photonics Society Publication

Invited Paper

Realization and Characterization of Aligned Silicon Nanowire Array With Thin Silver Film

Volume 3, Number 3, June 2011

Yung-Jr Hung, Member, IEEE
San-Liang Lee, Senior Member, IEEE
Kai-Chung Wu
Yen-Ting Pan

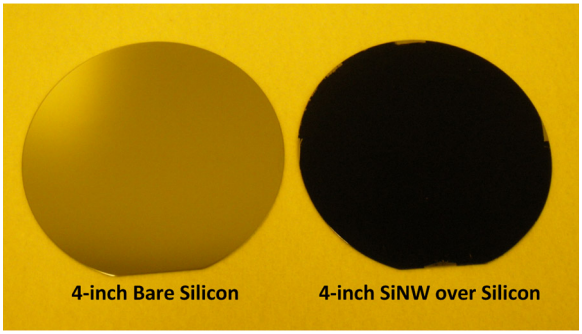

DOI: 10.1109/JPHOT.2011.2151277
1943-0655/$26.00 ©2011 IEEE

IEEE photonics SOCIETY
IEEE

Realization and Characterization of Aligned Silicon Nanowire Array With Thin Silver Film

Yung-Jr Hung, *Member, IEEE*, San-Liang Lee, *Senior Member, IEEE*, Kai-Chung Wu, and Yen-Ting Pan

(Invited Paper)

Department of Electronic Engineering, National Taiwan University of Science and Technology (NTUST), Taipei 106, Taiwan

DOI: 10.1109/JPHOT.2011.2151277

Manuscript received February 22, 2011; revised April 29, 2011; accepted April 29, 2011. Date of current version June 28, 2011. This work was supported by National Science Council, Taiwan, under Grant NSC97-2221-E-011-077-MY3 and the Ministry of Education, Taiwan, under the Top University Program. Corresponding author: Y.-J. Hung (e-mail: d9502307@mail.ntust.edu.tw).

Abstract: Wafer-scale fabrication of aligned and uniform silicon nanowire (SiNW) arrays is achieved with good controllability and reproducibility by depositing a thin silver film on a silicon surface prior to wet etching. Fast SiNW formation with a rate of 1.4 μm/min is achieved with optimized process condition, while lower etching rate enables finer SiNW formation in a small open area. Realized SiNWs are demonstrated to have good material and optical properties. With the help of aligned SiNWs, we demonstrate the fabrication of a black nonreflecting silicon surface with a surface reflectivity of around 2–4% uniformly over a 4-in wafer area. This material is expected to be promising as a building block for various applications due to its low-cost and mass-producible fabrication and excellent characteristics.

Index Terms: Engineered photonic nanostructures, subwavelength structures, fabrication and characterization.

1. Introduction

Silicon nanowire (SiNW) arrays have been extensively used as the building blocks for many emerging technologies, such as biomedical sensing [1], chemical sensing [2], transistors [3], solar cells [4]–[7], and thermoelectric devices [8]. Various bottom-up growth techniques have been developed to prepare silicon nanostructures [9]–[11]. However, these growth mechanisms have some limitations as they generally require complex and expensive equipment or employ hazardous silicon precursors. Except for bottom-up growth techniques, a sequence of patterning and etching processes are usually required to realize nanostructures in semiconductors. Most of nanostructures are patterned using electron-beam lithography, which has the disadvantages of being time consuming and low throughput. Most of etching processes require a hard mask for the following deep pattern transferring into silicon. Recently, we have realized tall and highly ordered SiNW arrays over a large sample area by using low-cost interference lithography and novel single-step deep reactive ion etching [12], [13]. With this novel etching process, patterned nanostructures can be transferred directly from resist template into silicon. Another big group of research focuses on SiNW realization by means of metal-induced chemical etching [14]–[19]. Disordered SiNW arrays can be realized by immersing clean silicon wafers in metal-contained aqueous solution, such as $HF/AgNO_3$ [14], [15],

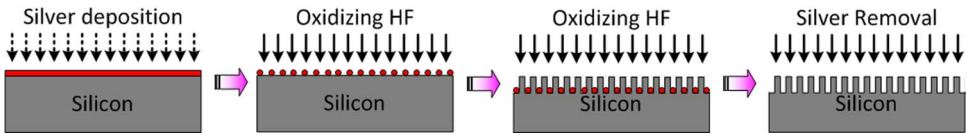

Fig. 1. Schematic diagram of the proposed fabrication process for realizing aligned SiNWs.

or by immersing metal-distributed silicon wafers in oxidizing hydrofluoric acid solution, such as HF/H_2O_2 [16], [17]. Silver or gold particles are deposited mostly by electroless plating process as the catalysts in this etching process. Simple, low-cost, and mass-producible fabrication is the obvious advantages of this method. However, agglomeration of the fabricated SiNWs usually takes place at the top surface, resulting in large voids and hence limiting its applications. This is partially due to the random electroless deposition of metal particles which have random sizes and locations. Although aligned and ordered SiNW arrays can be realized with metal-induced chemical etching, additional patterning processes such as nanosphere lithography or interference lithography are still necessary [18], [19]. In this paper, we present a much simplified fabrication process for synthesizing aligned and uniform SiNW arrays by simply depositing thin silver film on Si surface prior to wet chemical etching in oxidizing HF solution. By characterizing the material and optical properties, SiNWs with low reflection and good uniformity are feasible for applications in wafer-scale device fabrication.

2. SiNW Fabrication

The synthesis of aligned SiNW arrays is carried out on front-side polished, boron-doped (100) crystalline silicon wafers with a resistivity of 1–10 Ω-cm. Fig. 1 shows the schematic diagram of the proposed fabrication process, aiming to realize vertically aligned SiNW arrays. This process comprises three steps: 1) A thin silver film is deposited onto the cleaned Si surface by electron-beam evaporation with a low depositing rate; 2) the metal-treated Si wafers are immersed in oxidizing hydrofluoric acid solution for anisotropic wet chemical etching; and 3) the as-prepared samples are treated in nitric acid to completely remove the residual silver particles. The main idea of this fabrication process is to replace the randomly distributed silver particles in prior art [14]–[17] with network-like percolated silver film, thus allowing the formation of high-density SiNWs with uniform wire diameters. A similar idea was used in previous work to investigate the role of silver in metal-induced etching process [20], but the entire etching process needs to be optimized for obtaining aligned and uniform SiNW arrays.

Several experiments have been performed to investigate the effects of different process conditions. For comparisons, the reference process condition is set as the concentrations of HF, H_2O_2, and H_2O being 6.72 M, 0.79 M, and 48 M, respectively, initial silver thickness of 20 nm, and etchant temperature of 25 degree Celsius. The etchant composition ρ is defined as the molar ratio between the H_2O_2 and HF concentrations, that is, $\rho = [\mathrm{HF}]/([\mathrm{HF}] + [\mathrm{H_2O_2}])$. The etchant composition of the reference process condition is 0.89. Unless mentioned, all process parameters in the following experiments are based on the reference process condition. The resultant SiNW profiles are characterized by using a field-emission scanning electron microscope (SEM).

The thickness of silver film is critical to the success of high-quality SiNW formation since the morphology of thin silver film changes with the thickness from the initial nuclei/small grains (2–3 nm), percolated silver channel stage (3–22 nm) to completely continuous ($>$ 22 nm). It was reported that depositing a very thin layer of gold or platinum on Si prior to HF/H_2O_2 etching produces porous silicon [21]. We also find similar phenomenon for 5 nm thick silver film, as shown in Fig. 2(a). Since there are many gaps among thin metal clusters, random and disordered silicon etching happens in this case, and no SiNW is produced. Instead, porous silicon surface with a penetration depth of around 1.8 μm is realized after 5 min of etching. If the silver film is completely continuous, etched SiNW array is nonuniform because the paucity of gaps prevents the etching solution from contacting with the silicon. The silver film is lifted off at some places where no SiNW are formed, as

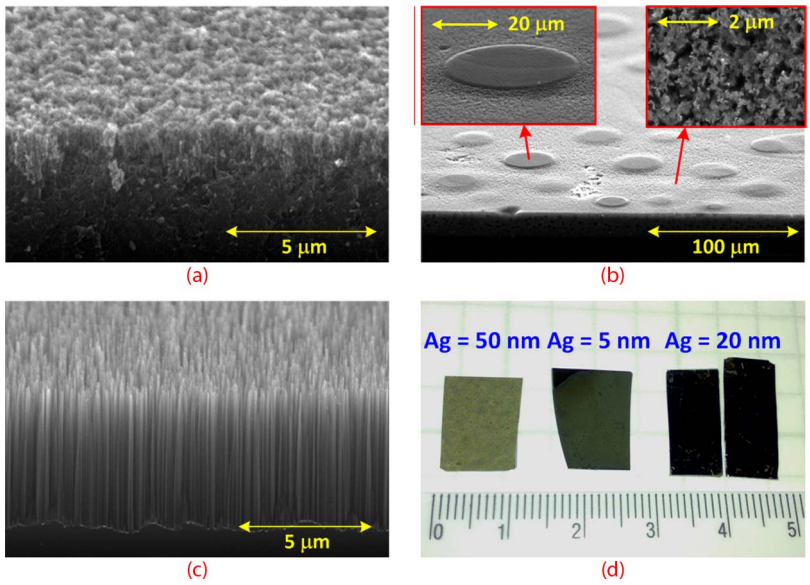

Fig. 2. Cross-sectional SEM pictures of (a) porous silicon surface realized with a silver thickness of 5 nm, (b) nonuniform rough surface realized with a silver thickness of 50 nm, and (c) vertical aligned silicon nanowires realized with a silver thickness of 20 nm. (d) 5-min etched samples with different silver thicknesses.

shown in Fig. 2(b). The experiments show that SiNWs can only be formed by etching with a properly interconnected silver film. Fig. 2(c) shows the SEM picture of resultant SiNWs with a silver thickness of 20 nm. 5.25 μm tall and aligned SiNW array is realized with a density of around 3.6×10^7 wires per square millimeter after 5 min of etching. The diameters of fabricated SiNWs range from 66 nm to 115 nm. Fig. 2(d) shows photographs of 5-min etched SiNW samples with different initial silver thicknesses. A black nonreflecting silicon surface is realized by the etching with 20 nm thick silver since the SiNWs are deep, aligned, and highly uniform over the entire sample area.

Except for silver thickness, silicon etching behavior of the proposed method is also determined by varying the etchant composition and etchant temperature. It was reported that high etchant composition $(1 > \rho > 0.7)$ leads to the formation of straight pores with diameter matching the size of the silver nanoparticles embedded at their bottom [17]. The highest silver penetration rate (up to 4 μm/min) happens for an etchant composition of around 0.7 to 0.8. The use of very high etchant composition $(\rho > 0.95)$ usually results in much lower SiNW etching rate ($\sim$0.72 μm/min for the case of $\rho = 0.96$ and $\sim$0.25 μm/min for the case of $\rho = 1$) [15], [16]. Fig. 3 shows the SEM pictures of realized SiNWs with different etchant compositions. We observe that the agglomeration of fabricated SiNWs happens for the case of lower etchant composition $(\rho = 0.68)$, as shown in Fig. 3(d) and (e). Thanks for the uniform and close-packed silver nanocluster film, the agglomerated SiNWs still look uniform with a cluster-to-cluster distance of only around 1 μm, as compared to that realized with conventional electroless fabrication method [15]. The experiments show that vertically aligned SiNW arrays can be reproducibly realized with an etchant composition of $\rho = 0.89$, as shown in Fig. 3(a)–(c). The etchant composition to have similar SiNW profiles ranges from 0.87 to 0.95. The as-fabricated SiNWs are highly uniform over the entire sample area.

Fig. 4(a) shows the variation of maximum SiNW height under different etching time. The etching rate is very stable ($\sim$1.4 μm/min at room temperature) such that the etching depth can be easily controlled. The realized SiNWs are uniform and vertically aligned at least until the SiNW is 40 μm tall, as indicated in Fig. 5(a)–(c). However, as the etching time exceeds 25 min (SiNW height $>$ 40 μm), silver penetration becomes nonuniform, and some silver nanoparticles even stop scratching silicon. Only a few silver particles left at the bottom after 60 min of etching, even though the maximum SiNW height reaches around 90 μm, as shown in Fig. 5(d). This may be

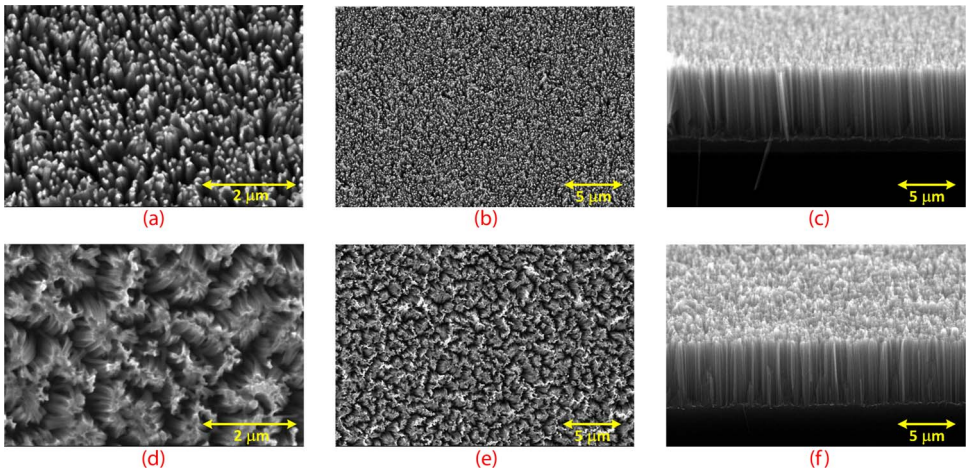

Fig. 3. SEM pictures of realized SiNWs with an etchant composition $[HF]/([HF] + [H_2O_2])$ of (a)–(c) 0.89 and (d)–(f) 0.68. The concentration of H_2O is fixed at 48 M. Etching time is fixed at 5 min.

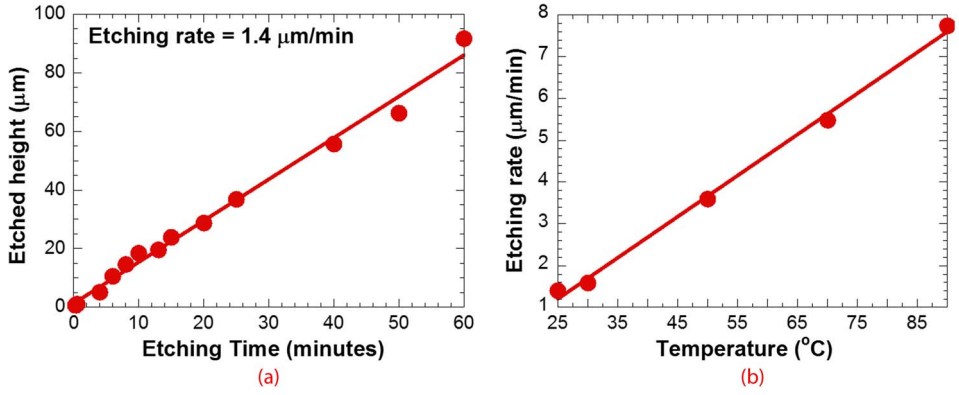

Fig. 4. (a) Etched SiNW height under different etching time in room temperature. (b) SiNW etching rate under different etchant temperatures.

partially due to the fact that the etching solution is hard to reach the bottom of high-aspect-ratio nanostructures, so the entire etching process slows down and finally stops. The etching rate can be further speeded up by increasing the etchant temperature with an increasing rate of around 89 nm/min/degree, as indicated in Fig. 4(b). However, an increased roughness on the top SiNW surface and SiNW-to-Si interface can be observed as the reaction is accelerated.

The capability of SiNW formation at designated places or within specific areas is important for applying this material to wafer-scale device fabrication, but most of the metal-induced etching processes reported in the literatures focuses on the SiNW realization on the top of blank silicon substrate. It was found to obtain better solar cell performance with the help of patterned SiNWs [7]. Therefore, the characterization of pattern effects to the SiNW formation is necessary. In this paper, a thin resist template is used as the etching mask. The pattern is designed to have different open widths ranging from 10 μm to 500 μm. Fig. 6(a) shows the variation of SiNW etching rate and total etching rate under different open widths and H_2O molar concentration. The SiNW etching rate and total etching rate are indicated in Fig. 6(d). In this experiment, higher etchant composition $(\rho = 0.93)$ is used to obtain slightly lower etching rate, which enables finer SiNW formation in a small open area. We observe that the difference between the SiNW and total etching rate is about $0.2 \sim 0.4$ μm/min for the case of less H_2O concentration $(H_2O = 48.3\ M)$ in the etchant. On the

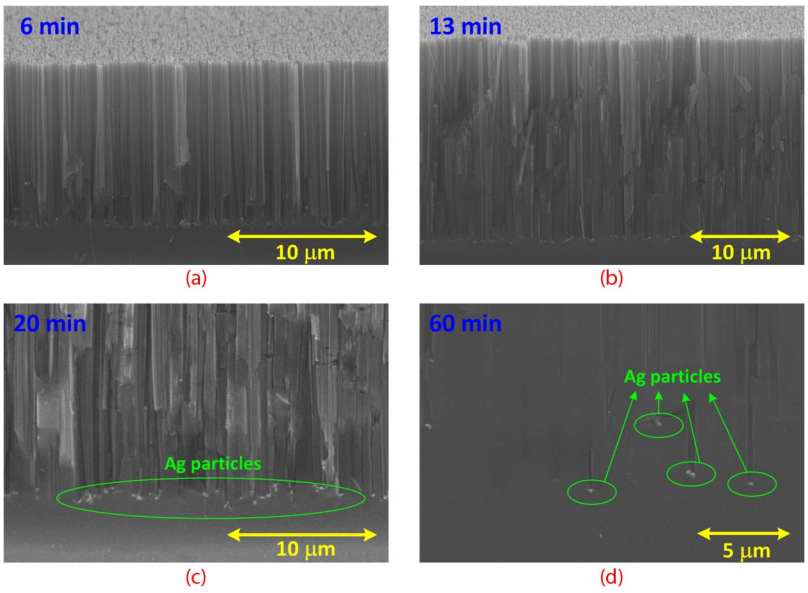

Fig. 5. Cross-sectional SEM pictures of realized SiNWs with an etching time of (a) 6 min, (b) 13 min, (c) 20 min, and (d) 60 min. (c) and (d) Enlarged images of the bottom of as-realized SiNWs after 20 and 60 min of etching, respectively. The whole etching process is carried out at room temperature.

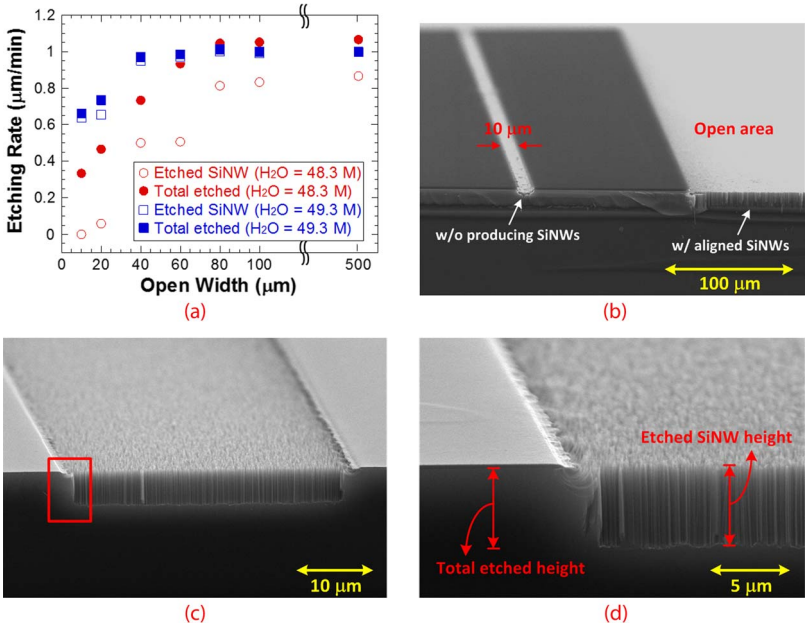

Fig. 6. (a) Variation of SiNW and total etching rate under different open widths. (b) Etched profile for different mask open areas. With much concentrated etchant ($H_2O = 48.3$ M), no SiNW is produced within a 10-μm wide open area. (c) Etched profile for 40-μm wide open area. More diluted etchant ($H_2O = 49.3$ M) is used in this experiment. (d) Enlarged image of rectangular box shown in plot (c). Lateral SiNW formation is found in the edge of mask.

contrary, there is almost no difference between SiNW and total etching rate with more diluted etchant ($H_2O = 49.3$ M). The results indicate that faster etching rate leads to more flood silicon removal in the beginning of etching. Besides, the SiNW etching rate, as well as the total etching

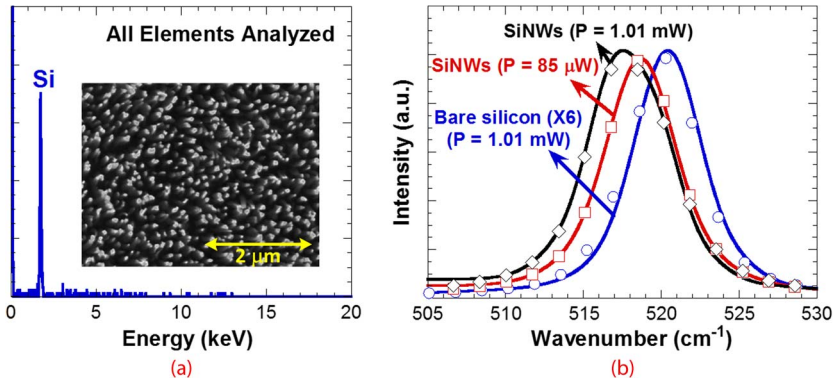

Fig. 7. (a) EDX spectrum of resultant SiNWs. (b) Raman spectra of bare silicon and 3-min etched SiNWs under different laser power.

rate, decreases as the open width becomes smaller. There is no SiNW produced within a 10-μm wide area, as shown in Fig. 6(b). With more diluted etchant $(H_2O = 49.3\ M)$, the SiNW etching rate within the 10-μm wide area is still about 0.65 μm/min. We find that the SiNW etching rate within a 40-μm wide area is about the same as that within entire open area, as shown in Fig. 6(c). The realized SiNWs are still uniform and vertically aligned over the entire open area. Fig. 6(d) is the zoom-in of the enclosed area in Fig. 6(c). Fig. 6(d) also indicates that lateral SiNW formation happens on the edge of masked areas. Similar results were also obtained in previous study [19]. We believe that every silver nanoparticle can catalyze the etching of contacted silicon freely in random downward directions. This is also the reason why very thin metal films could produce porous silicon surface [21]. Due to the network-like silver nanoclusters which restrict each silver nanoparticle to move freely, collective sinking of silver nanoparticles in downward direction happens in open areas, resulting in the formation of vertically aligned SiNWs.

3. Material Characterization

We performed the Raman spectroscopy and energy-dispersive X-ray spectroscopy (EDX) measurement to characterize the structural and chemical properties of fabricated SiNW arrays. The measured EDX spectrum of resultant SiNWs shown in Fig. 7(a) confirms that nanowires are purely made of silicon, and no trace of metallic impurities such as silver is observed. Raman spectroscopy is an important technique for nondestructive structural characterization of SiNWs. It has been observed in SiNWs the downshift and broadening of Raman spectra due to the phonon confinement effects [22]–[25]. Such effects are observable only for structures with at least one of the three main dimensions smaller than 15 nm. On the contrary, the spectral changes in Raman spectra of SiNWs with larger diameters are attributed to the intense local thermal heating caused by the pumping laser [25]. As the local temperature of SiNWs increases, the lattice constant increases, and the bonds between atoms weaken, thus broadening the Raman line of SiNWs asymmetrically, which can be well fit by a Fano resonance line shape that is associated with an interfering continuum scattering process activated by the incident laser irradiation [24]. The heating of the nanowire can be exaggerated by poor thermal resistance of the nanowires and tight focusing of the incident laser beam. The local temperature in the SiNWs is approximately linear with the incident laser power and could be as high as 400 $\sim$ 500 K for a laser power of $\sim$1 mW [24]. This local heating phenomenon is peculiar to nanostructures and is generally not observed in bulk silicon.

The Raman spectra for bulk silicon and SiNWs realized by the proposed fabrication method are shown in Fig. 7(b). The spectra for excitation with different laser powers are also shown for comparison. The laser wavelength is fixed at 514 nm. Ten times longer integrating time is used for Raman characterization with lower laser power (P = 85 μW, corresponding to a power density of 4.3×10^6 W/m^2) to obtain almost the same energy as that with higher laser power (P = 1.01 mW,

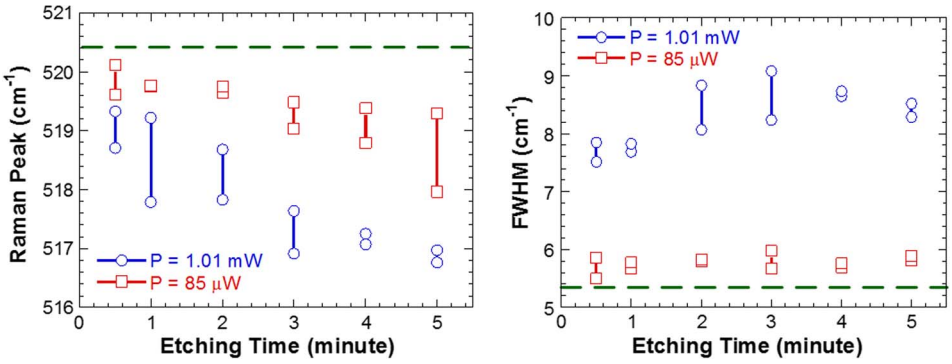

Fig. 8. (a) Peak and (b) FWHM of Raman spectra of resultant SiNWs under different laser power and SiNW etching time. Dashed line indicates the case for original p-type silicon.

corresponding to a power density of 5×10^7 W/m^2). Enhanced Raman intensity of SiNWs is observed as compared to that of bulk silicon due to the increased transmitted excitation intensity into the SiNW material [15]. Since the dimension of realized SiNWs is large in diameter (initially 66 nm to 115 nm in most area; decreases with the etching time) and length (half micrometer to tens of micrometers), the main reason to the spectral changes of high-power (1.01 mW) irradiated SiNWs is attributed to much increased local temperature in SiNWs. A small phonon band shift of $\sim$1 cm^{-1} and a full-width at half-maximum (FWHM) broadening of only 0.4 cm^{-1} are also observed in 84-μW irradiated SiNWs. We still attribute this phenomenon to small amount of elevated local temperature in SiNWs caused by laser.

Fig. 8 shows the peak and FWHM of Raman spectra for the SiNWs of different etching time under different laser power excitation. The dashed line indicates the case for original p-type silicon. A larger downshifted and broad peak can be observed for the excitation with higher laser power, especially for the changes in FWHM values. As the SiNWs are taller (longer etching time), the Raman peak of SiNWs moves further to lower frequencies while its FWHM value remains almost the same. Since the SiNWs become taller and slightly smaller with the increasing etching time, we attribute the spectral changes to the increased local temperature in SiNWs due to the low thermal conductivity of tall and smaller SiNWs as well as the poor thermal contact with the substrate [8].

4. Optical Characterization

Nanostructures can be used as a surface antireflection layer for improving the performance of many optical and optoelectronic devices [4]–[7]. SiNW arrays realized by conventional electroless silver deposition and wet chemical etching were found to provide good antireflective properties [26]. However, as mentioned above, the wire agglomeration due to random deposition of silver nanoparticles results in large voids and thus degrades the antireflective properties [15]. Besides, unlike the conventional scheme requiring critical control of the chemical solution, our approach is relatively simple and advantageous for realizing uniform SiNWs over large area because it only requires deposition of a thin silver film. Fig. 9 shows the photograph of the fabricated SiNWs over 4-in wafer area. The SiNW sample appears totally black with good uniformity, as compared to the gray and polished surface of original silicon substrate. This verifies low surface reflection over the whole 4-in SiNW sample.

Optical reflection and transmission of SiNW sample is measured for the spectral regions above and below the bandgap of silicon with a spectrophotometer (JASCO UV–Vis/NIR spectrophotometer V-670) equipped with an integrating sphere. Fig. 10(a) shows the comparison of optical reflection between bare silicon and 5-μm tall SiNWs. In the Si absorption region, the reflection spectrum of original bare silicon shows the typical high reflectivity of the front polished surface. The higher reflectivity below the fundamental absorption bandgap E_{gap} of silicon is due to the additional diffuse reflection from the back silicon surface. After realizing 5-μm tall SiNWs on the top, the total

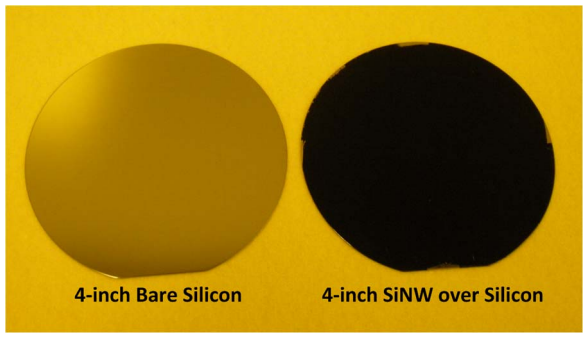

Fig. 9. Original bare silicon and aligned SiNWs on silicon. Realized SiNWs are highly uniform over 4-in silicon wafer area.

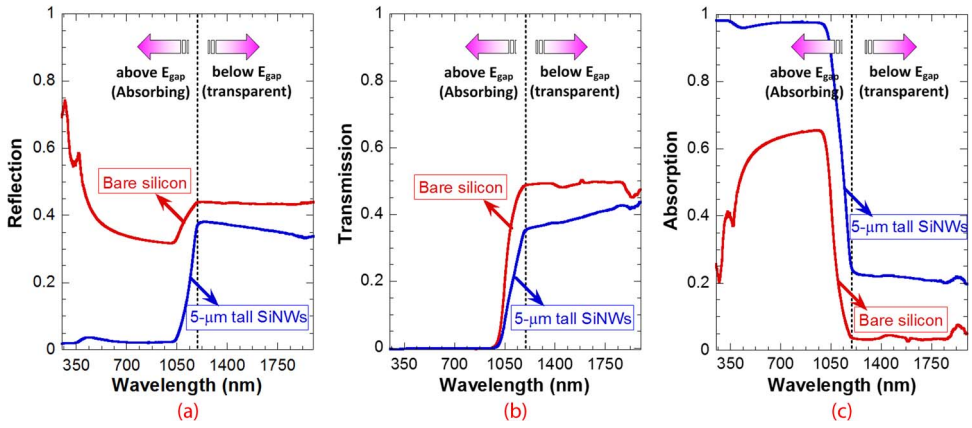

Fig. 10. Comparison of (a) optical reflection, (b) optical transmission, and (c) optical absorption between bare silicon and 5-μm tall SiNWs.

surface reflectivity in the spectral region above E_{gap} has decreased down to around 2–4%. The net internal absorption A is calculated from the corresponding reflection R and transmission T according to $R + T + A = 1$. With the help of SiNWs, the amount of absorbed light is significantly increased from below 0.65 to above 0.96 in the entire Si absorbing region, as shown in Fig. 10(c). However, in the Si transparency region, the decreased reflection of the SiNW surface is not accompanied by a corresponding increase of transmitted light but leads to even lower optical transmission as compared to that of bare silicon, as shown in Fig. 10(b). It indicates that there is strong residual absorption below the Si bandgap in 5-μm tall SiNWs. We attribute this residual absorption to strong infrared light trapping coupled with the presence of surface states on the nanowires that absorb below bandgap light. This subbandgap absorption also occurred in microstructured silicon [27] and can be slightly decreased with post annealing process [27], [28].

5. Conclusion

We demonstrate a simple fabrication approach to realize aligned, high-density, and uniform SiNW array by depositing thin silver film on Si surface prior to wet chemical etching in oxidizing HF solution. The main idea of this fabrication process is to replace randomly distributed silver particles with network-like percolated silver film as the catalyst for SiNW formation, trying to avoid the agglomeration issue which usually happens in the conventional electroless deposition scheme. The control of silver thickness and etchant composition is the key to the success of this fabrication approach. With a silver thickness of 20 nm and an etchant composition of 0.89, high-quality SiNW

arrays are realized with good reproducibility and controllability. The SiNW etching rate is fast ($\sim$1.4 μm/min) and stable and can be further speeded up by lifting the etchant temperature such that the etching depth can be easily controlled. We also developed the etching conditions for a lower etching rate to enable finer SiNW formation in small open area.

The EDX characterization has confirmed that nanowires are purely made of silicon; and no trace of metallic impurities such as silver is observed. Downshifted and broad Raman peak is also found in realized SiNWs which is attributed to the local laser heating effect. This phenomenon is even obvious in taller and smaller SiNW due to its poor thermal conductivity. The fabricated SiNWs are very effective in reducing the surface reflection of silicon samples over a broad spectral region. We demonstrate the fabrication of aligned SiNWs with black and uniform surface over 4-in wafer area. Around 2–4% total surface reflection in above-bandgap spectral region is obtained with 5-μm tall SiNWs. The proposed approach is feasible for mass production of high-quality SiNWs for various applications.

Acknowledgment

The authors would like to thanks Prof. Y.-S. Huang of the Department of Electronic Engineering, NTUST, and Prof. Y. Tai of the Department of Chemical Engineering, NTUST, and their students for their help with Raman and optical characterization.

References

[1] B. R. Murthy, J. K. K. Ng, E. S. Selamat, N. Balasubramanian, and W. T. Liu, "Silicon nanopillar substrates for enhancing signal intensity in DNA microarrays," *Biosens. Bioelectron.*, vol. 24, no. 4, pp. 723–728, Dec. 2008.
[2] A. A. Talin, L. L. Hunter, F. Leonard, and B. Rokad, "Large area, dense silicon nanowire array chemical sensors," *Appl. Phys. Lett.*, vol. 89, no. 15, pp. 153102-1–153102-3, Oct. 2006.
[3] J. Goldberger, A. I. Hochbaum, R. Fan, and P. Yang, "Silicon vertically integrated nanowire field effect transistors," *Nano Lett.*, vol. 6, no. 5, pp. 973–977, May 2006.
[4] Z. Fan, D. J. Ruebusch, A. A. Rathore, R. Kapadia, O. Ergen, P. W. Leu, and A. Javey, "Challenges and prospects of nanopillar-based solar cells," *Nano Res.*, vol. 2, no. 11, pp. 829–843, Nov. 2009.
[5] Y.-J. Hung, S.-L. Lee, and L. A. Coldren, "Deep and tapered silicon photonic crystals for achieving anti-reflection and enhanced absorption," *Opt. Exp.*, vol. 18, no. 7, pp. 6841–6852, Mar. 2010.
[6] C. Chen, R. Jia, H. Yue, H. Li, X. Liu, D. Wu, W. Ding, T. Ye, S. Kasai, H. Tamotsu, J. Chu, and S. Wang, "Silicon nanowire-array-textured solar cells for photovoltaic application," *J. Appl. Phys.*, vol. 108, no. 9, pp. 094318-1–094318-5, Nov. 2010.
[7] D. Kumar, S. K. Srivastava, P. K. Singh, M. Husain, and V. Kumar, "Fabrication of silicon nanowire arrays based solar cell with improved performance," *Sol. Energy Mater. Sol. Cells*, vol. 95, no. 1, pp. 215–218, Jan. 2011.
[8] A. I. Hochbaum, R. Chen, R. D. Delgado, W. Liang, E. C. Garnett, M. Najarian, A. Majumdar, and P. Yang, "Enhanced thermoelectric performance of rough silicon nanowires," *Nature*, vol. 451, no. 7175, pp. 163–167, Jan. 2008.
[9] J. Bauer, F. Fleischer, O. Breitenstein, L. Schubert, P. Werner, V. Gosele, and M. Zacharias, "Electrical properties of nominally undoped silicon nanowires grown by molecular-beam epitaxy," *Appl. Phys. Lett.*, vol. 90, no. 1, pp. 012105-1–012105-3, Jan. 2007.
[10] H. Pan, S. Lim, C. Poh, H. Sun, X. Wu, Y. Feng, and J. Lin, "Growth of Si nanowires by thermal evaporation," *Nanotechnol.*, vol. 16, no. 4, pp. 417–421, Apr. 2005.
[11] K. K. Lew and J. M. Redwing, "Growth characteristics of silicon nanowires synthesized by vapor-liquid-solid growth in nanoporous alumina templates," *J. Cryst. Growth*, vol. 254, no. 1/2, pp. 14–22, Jun. 2003.
[12] Y.-J. Hung, S.-L. Lee, B. J. Thibeault, and L. A. Coldren, "A novel approach for realizing highly-ordered silicon nanopillar arrays with a high aspect ratio and controllable sidewall profiles," presented at the Materials Res. Soc. (MRS) Meeting, San Francisco, CA, 2010, Paper Q14-02.
[13] Y.-J. Hung, S.-L. Lee, B. J. Thibeault, and L. A. Coldren, "Fabrication of highly-ordered silicon nanowire arrays with controllable sidewall profiles for achieving low surface reflection," *IEEE J. Sel. Topics Quantum Electron.*, DOI: 10.1109/JSTQE.2010.2068540, to be published.
[14] T. Qiu, X. L. Wu, G. G. Siu, and P. K. Chu, "Intergrowth growth mechanism of silicon nanowires and silver dendrites," *J. Electron. Mater.*, vol. 35, no. 10, pp. 1879–1884, Oct. 2006.
[15] D. Kumar, S. K. Srivastava, P. K. Singh, K. N. Sood, V. N. Singh, N. Dilawar, and M. Husain, "Room temperature growth of wafer-scale silicon nanowire arrays and their Raman characteristics," *J. Nanopart. Res.*, vol. 12, no. 6, pp. 2267–2276, 2010.
[16] K. Peng, A. Lu, R. Zhang, and S._T. Lee, "Motility of metal nanoparticles in silicon and induced anisotropic silicon etching," *Adv. Funct. Mater.*, vol. 18, no. 19, pp. 3026–3035, Oct. 2008.
[17] C. Chartier, S. Bastide, and C. Levy-Clement, "Metal-assisted chemical etching of silicon in HF-H_2O_2," *Electrochim. Acta*, vol. 53, no. 17, pp. 5509–5516, Jul. 2008.
[18] Z. Huang, H. Fang, and J. Zhu, "Fabrication of silicon nanowire arrays with controlled diameter, length, and density," *Adv. Mater.*, vol. 19, no. 5, pp. 744–748, Mar. 2007.

[19] W. K. Choi, T. H. Liew, M. K. Dawood, H. I. Smith, C. V. Thompson, and M. H. Hong, "Synthesis of silicon nanowires and nanofin arrays using interference lithography and catalytic etching," *Nano Lett.*, vol. 8, no. 11, pp. 3799–3802, Nov. 2008.
[20] H. Fang, Y. Wu, J. Zhao, and J. Zhu, "Silver catalysis in the fabrication of silicon nanowire arrays," *Nanotechnol.*, vol. 17, no. 15, pp. 3768–3774, Aug. 2006.
[21] X. Li and P. W. Bohn, "Metal-assisted chemical etching inHF/H_2O_2 produces porous silicon," *Appl. Phys. Lett.*, vol. 77, no. 16, pp. 2572–2574, Oct. 2000.
[22] B. Li, D. Yu, and S.-L. Zhang, "Raman spectral study of silicon nanowires," *Phys. Rev. B*, vol. 59, no. 3, pp. 1645–1648, Jan. 1999.
[23] S. Piscanec, A. C. Ferrari, M. Cantoro, S. Hofmann, J. A. Zapien, Y. Lifshitz, S. T. Lee, and J. Robertson, "Raman spectrum of silicon nanowires," *Mater. Sci. Eng. C*, vol. 23, no. 6–8, pp. 931–934, Dec. 2003.
[24] R. Gupta, Q. Xiong, C. K. Adu, U. J. Kim, and P. C. Eklund, "Laser-induced Fano resonance scattering in silicon nanowires," *Nano Lett.*, vol. 3, no. 5, pp. 627–631, May 2003.
[25] S. Piscanec, M. Cantoro, A. C. Ferrari, J. A. Zapien, Y. Lifshitz, S. T. Lee, S. Hofmann, and J. Robertson, "Raman spectroscopy of silicon nanowires," *Phys. Rev. B*, vol. 68, no. 24, pp. 241312-1–241312-4, Dec. 2003.
[26] S. K. Srivastava, D. Kumar, P. K. Singh, M. Kar, V. Kumar, and M. Husain, "Excellent antireflection properties of vertical silicon nanowire arrays," *Sol. Energy Mater. Sol. Cells*, vol. 94, no. 9, pp. 1506–1511, Sep. 2010.
[27] C. Wu, C. H. Crouch, L. Zhao, J. E. Carey, R. Younkin, J. A. Levinson, E. Mazur, R. M. Farrell, P. Gothoskar, and A. Karger, "Near-unity below-band-gap absorption by microstructured silicon," *Appl. Phys. Lett.*, vol. 78, no. 13, pp. 1850–1853, Mar. 2001.
[28] L. Tsakalakos, J. Balch, J. Fronheiser, M.-Y. Shih, S. F. LeBoeuf, M. Pietrzykowski, P. J. Codella, B. A. Korevaar, O. Sulima, J. Rand, A. Davuluru, and U. Rapol, "Strong broadband optical absorption in silicon nanowire films," *J. Nanophoton.*, vol. 1, no. 1, pp. 013552-1–013552-10, Jul. 2007.